



# Applied Mathematics and Nonlinear Sciences

<https://www.sciendo.com>

## The Triaxiality Role in the Spin-Orbit Dynamics of a Rigid Body

A. Cantero<sup>1†</sup>, F. Crespo<sup>2</sup>, S. Ferrer<sup>1</sup>

1 DITEC, Facultad de Informática, Universidad Murcia, 30071 Espinardo, Murcia  
Spain

2 GISDA, Dept. de Matemática, Facultad de Ciencias, Universidad del Bío-Bío, Collao 1202, Casilla 5-C.  
Concepción Chile

---

### Submission Info

Communicated by Juan L.G. Guirao

Received 6th February 2018

Accepted 21th May 2018

Available online 21th May 2018

---

### Abstract

We study the roto-orbital dynamics of a uniform sphere and a triaxial body by means of a radial intermediary, which defines a 2-DOF Hamiltonian system. Our analysis is carried out by using variables referred to the total angular momentum. Its validity and applicability is assessed numerically by experiments comprising three different scenarios; analysis of the triaxiality, eccentricity and altitude. They show that there is a range of parameters and initial conditions for which the radial distance and the slow angles are estimated accurately, even after one orbital period. On the contrary, fast angles deteriorates as the triaxiality grows. We also include the study of the relative equilibria, finding constant radius solutions filling 4-D and lower dimensional tori. These families of relative equilibria include some of the classical ones reported in the literature and some new types. For a number of scenarios the relation between the triaxiality and the inclination connected with relative equilibria are given.

---

**Keywords:** Rotational and orbital dynamics, gravity-gradient, intermediary, relative equilibria

**AMS 2010 codes:** 70F05, 70F15.

---

### List of symbols

$A_1, A_2, A_3,$	Principal moments of inertia
$\alpha$	Triaxiality parameter $\alpha = 2A_3 - A_1 - A_2$
$\mathbf{b}_i$	Body frame vectors
$\mathcal{B}_i$	Body with mass $m_i$
$\mathbf{E}_i$	Spatial frame vectors
$\mathcal{G}$	Universal gravitational constant

---

<sup>†</sup>Corresponding author.

Email address: [antonio.cantero@um.es](mailto:antonio.cantero@um.es)

$\mathbf{G}, \mathbf{G}_o, \mathbf{G}_r$	Total, orbital, rotational angular momentum vectors in body frame
$G, G_o, G_r$	Modulus of the corresponding vectors
$h$	Argument of the node relative to the orbital plane
$\mathcal{H}$	Hamilton function of the intermediary model
$\mathcal{H}_K$	Kepler system
$\mathcal{H}_E$	Free rigid body
$\mathcal{H}_0$	Zero order Hamiltonian ( $\mathcal{H}_0 = \mathcal{H}_K + \mathcal{H}_E$ )
$\mathcal{H}_1$	Perturbation
$I_o$	Angle between $\Pi_o$ and $\Pi$
$I_r$	Angle between $\Pi_r$ and $\Pi$
$I$	Inclination of the total angular momentum plane
$I_\Delta$	Inclination of the rotational plane
$I_\Theta$	Inclination of the orbital plane
$l$	Node of the total angular momentum plane
$l_I$	Body plane (see $\Pi_b$ ) and rotational planes intersection
$l_r, -l_o$	Total, orbital and rotational planes intersection
$l_{\mu\delta}$	Rotational and spatial planes intersection
$l_\theta$	Orbital and spatial planes intersection
$M$	Total mass of the system
$m$	Reduced mass of the system
$m_i$	Mass of the body $\mathcal{B}_i$
$\mathbf{n}$	Unitary vector parallel to the total angular momentum
$N, N'$	Third component of $\mathbf{G}_r$
$\mathcal{P}$	Gravitational potential
$\mathbf{p}$	Linear momentum associated to $\mathbf{r}$
$q$	$m/m_1$
$r, r'$	Modulus of the vector joining the mass center of the bodies
$\mathbf{r}$	Vector joining the mass center of the bodies
$R, R'$	Radial velocity of the center of mass
$R_1$	Distance between the center of mass and the furthest point of $\mathcal{B}_1$
$R_2$	Distance between the center of mass and the furthest point of $\mathcal{B}_2$
$\mathbf{R}_i$	Position vector of the body $\mathcal{B}_i$ in the inertial frame
$U$	MacCullagh's term
$\mathcal{V}$	Potential of the intermediary model
$\gamma_i$	Direction cosines of $\mathbf{r}/r$
$\delta, \delta'$	Argument of the angle between $l_r$ and $l_I$
$\Delta, \Delta'$	Magnitude of the angular momentum of the rigid body
$\theta, \theta'$	Argument of the vector joining the center of masses of the two bodies
$\Theta, \Theta'$	Magnitude of the angular momentum of the center of mass
$\iota$	$I_o + I_r$
$\kappa$	$\mathcal{G}M$
$\lambda$	Argument of the node relative to the Andoyer plane
$\mu, \mu'$	Argument of the angle between $l_{\mu\delta}$ and $l_I$
$\nu, \nu'$	Argument of the angle between $l_I$ and $b_1$
$\mathbf{\Pi}$	Angular momentum of the body $\mathbf{B}_1$
$\rho$	Triaxiality parameter
$\Pi$	Total angular momentum plane
$\Pi_b$	Body plane, $\mathbf{b}_1\mathbf{b}_2$ -plane
$\Pi_o$	Orbital plane
$\Pi_r$	Andoyer plane
$\sigma$	Angle between $\Pi_r$ and the body plane
$\tau_1$	Triaxiality ratio of $A_1$ and $A_3$
$\tau_2$	Triaxiality ratio of $A_2$ and $A_3$
$T_O$	Orbital kinetic energy
$T_R$	Rotational kinetic energy
$\phi, \phi'$	Argument of the node of the total angular momentum plane
$\Phi, \Phi'$	Third component of the total angular momentum in space frame
$\psi, \psi'$	Argument of $l_r$
$\Psi, \Psi'$	Magnitude of the total angular momentum

## 1 Introduction

The full gravitational 2-body problem (FG2BP) accounts for the dynamics of two rigid bodies  $\mathcal{B}_1$  and  $\mathcal{B}_2$ , with masses  $m_1$  and  $m_2$ , which mutual interaction is exclusively originated by gravitational attraction. In a previous work [11], we focussed on an axis-symmetric approximation. Here, our main goal is to figure out how this modelization is influenced by the assumption of a triaxial body in the absence of spin-orbit resonances.

The FG2BP is far from being well understood and requires physical and mathematical simplifications to be tackled, [27]. Therefore, only partial approaches are possible by now. The strongest streamlining of the FG2BP is carried out by assuming two point masses, then leading to the Kepler system by setting the Jacobi coordinates. A possible generalisation of this situation keeping the integrability is assuming two spherical masses. Thus, obtaining Keplerian motion for the orbital part, which is independent of the uniform rotation of the two spheres. Next level in the generalisation of the ideal situation is to consider an asymmetric body and a sphere of homogeneous density. Nevertheless, this situation still leads to a wide set of scenarios depending on the distances and masses involved. For instance, truncation of the gravitational potential associated to this problem up to the second order, the so called MacCullagh's approximation, is possible when the orbiting body is small compared with the distance between the mass centres. In our work, we precisely consider this situation and discard terms on the gravitational potential higher than two. As such, from now on we will refer indistinctly to this approximation as the MacCullagh's truncation and the full model as well. A different story would be if we considered two generic bodies, then the fourth order of the gravitational potential includes terms of the body-body interaction and not only spin-orbit interaction, as it happens with the second order term. Therefore, the truncation of the potential in this case is recommended at least to the fourth order, see [4].

The study of the attitude dynamics of a generic triaxial spacecraft in a central gravitational field permeates along the space era, from [3], [7], [8] and [22], up to the very recent research including [12], [28] and [31]. This problem covers aspects such as determination, propagation and control, that continue to be areas of research, see [20, 29, 33] for further details. Common to these studies has been the assumption of fast rotation. Hence, distinguishing between fast and slow variables, rotational motion has been approached by perturbative techniques [24].

We approach the gravity-gradient problem making use of the concept of *intermediary*, which has long tradition in both astronomy and astrodynamics. More precisely, following Poincaré and Arnold, we split the Hamiltonian into two terms:

$$\mathcal{H} = \mathcal{H}_0 + \mathcal{H}_1,$$

where the intermediary  $\mathcal{H}_0$  defines a non-degenerate and simplified model of the problem at hand, which includes the Kepler and free rigid-body as particular cases and  $\mathcal{H}_1$  is usually dubbed as the perturbation. A special realization of an intermediary occurs for the case in which it is an integrable 1-DOF system. The work of Hill on the Moon motion [32] is, perhaps, the best known example. The interest on an intermediary is twofold. On the one hand, it allows us to identify special solutions that could become nominal trajectories in missions design whereas it alleviates usual heavy computations. On the other hand, it can be used to build a perturbation theory based on a new unperturbed part avoiding the degenerate character inherent to the classical superintegrable models (Kepler or free rigid body systems in astrodynamics). In other words, a first order perturbed solution based on intermediaries might be accurate enough for tracking purposes. In astrodynamics, when dealing with orbital dynamics applied to artificial satellites, some lines of research on intermediaries arose during the seventies by Garfinkel, Aksnes, Cid, Sterne, etc. (see review in [14]), whose benefits are now seen in areas such as the relative motion in formation flights, an example is given in [25]. Nevertheless, less work has been done when dealing with attitude dynamics, where the proposal of intermediaries is more recent [2, 17] and, to our knowledge, no systematic study has been done on them.

In this paper, we continue our work on the intermediary model proposed in previous works [11, 19, 30], where an integrable 1-DOF intermediary was obtained by an uncontrolled truncation of the MacCullagh approximation [26] and assuming the secondary body to be in a Keplerian orbit. The accuracy of this model was tested by

comparing with the MacCullagh's truncation and showing a good performance in the numerical experiments. In our preceding work, we restrict to the study of the axis-symmetric case. The present manuscript complements this analysis by extending it to the case of a triaxial body and keeping all the remaining assumptions made previously. This change leads us to a 2-DOF intermediary model, which is expressed with variables referred to the total angular momentum, see [15, 17].

The validity and applicability of the model is assessed numerically. For that purpose, we study the accuracy of simulation in three different scenarios. First, we consider the triaxiality parameter introduced in [10],  $\rho = (A_2 - A_1)/(2A_3 - A_2 - A_1)$ . For  $\rho > 0$  the fast angles deteriorate very early and they are only well approximated for nearly zero values of  $\rho$ , though a detailed analysis for the case of a slow rotating body is still required. However, the radial distance and slow angles show a good performance for one orbital evolution. Precisely, radial error ratio  $(r_{Interm} - r_{full})/r_0$  is under 0.00064% and for the slow angles, we obtain differences up to the order  $10^{-6}$  radians. Secondly, we also take into account simulations for different eccentricities up to 0.5. As it is expected, approximations become worse as eccentricity grows. Finally, this behavior is reversed in the analysis of the altitude. Namely, as height grows the influence of the higher order terms in  $1/r$  is smaller. Hence, accuracy is improved by increasing height.

We also include the study of the relative equilibria, finding constant radius solutions filling a 4-D torus. In addition, equilibria leading to lower dimensional torus are identified and conditions for periodic orbits are detected. The intermediary model is endowed with several distinguishing and physical parameters. That is to say, physical constants are related to the bodies' features and integrals are characterized by their initial configuration. Having a high multidimensional parametric space introduces complexity in the study of bifurcations. With the aim of simplifying this scenario, we consider  $\cos \iota$ ,  $\cos \sigma$  and the set of principal moments of inertia  $(A_1, A_2, A_3)$  as the key objects to present the analysis of the relative equilibria. We will show that the evolution of  $\cos \iota \in [-\sqrt{1/3}, \sqrt{1/3}]$  allows for the appearance of the families dubbed as critical inclination equilibria ( $\cos \iota = \pm\sqrt{1/3}$ ) and  $\cos \iota$  leads to the body-perpendicular and body-inclined types. In our analysis, we find families that depart from the classical equilibria of the free rigid body and the classical equilibria reported in [16, 21]. Though, some of these equilibria are recovered in our setting.

This paper is organized as follows. Section 2 is devoted to introduce the triaxial intermediary into the Hamiltonian formalism and to describe the canonical variables in which it is expressed. In Section 3, we present the numerical simulations bounding the applicability and validity of the model. In addition, conditions leading to families of relative equilibria are identified in Section 4. We establish the connection of our families of relative equilibria with the classical ones reported in the related literature in Section 5. Finally, we present conclusions and include an Appendix section.

## 2 Hamiltonian formulation of the triaxial model

The formulation of the triaxial intermediary model follows the same derivation as the one made in [11], which is based in six simplifying assumptions. More specifically, the following set of simplifications are assumed in order to define our modelization: (i) *Barycentric coordinates*. The inertial frame is chosen to be moving with the total center of mass. (ii) *Shape and mass distribution of  $\mathcal{B}_2$* . The main body  $\mathcal{B}_2$  (mass  $m_2$ ) is endowed with spherical symmetry. (iii) *Size ratios*. Dimensions of the secondary body  $\mathcal{B}_1$  are small when compared to the distance between the centers of mass of the two bodies. (iv) *Shape and mass distribution of  $\mathcal{B}_1$* . The secondary body may be approximated by an homogeneous triaxial ellipsoid with total mass  $m_1$ . (v) *Eccentricity*. Only small eccentricity orbits are considered. (vi) *Resonances*. The case of spin-orbit resonances is not considered.

The Hamiltonian of the roto-orbital model is obtained from the mechanic energy function. Thus, denoting  $T_O$ ,  $T_R$  the orbital and rotational kinetic energies and  $\mathcal{P}$  the potential, the Hamiltonian function is defined in the

cotangent bundle of the special Euclidean group  $T^*SE(3)$

$$\begin{aligned}\mathcal{H} &= T_O + T_R + \mathcal{P} \\ &= T_O + T_R - \frac{\mathcal{G}M}{r} + \mathcal{V} \\ &= \mathcal{H}_K + \mathcal{H}_R + \mathcal{V},\end{aligned}\quad (1)$$

in other words, the potential is usually split in two parts: a term which depends only on  $1/r$  and  $\mathcal{V}$ , called the perturbing potential, depending on the rest of the variables of the problem. As a result, we have that  $\mathcal{H}_K = T_O - \mathcal{G}M/r$  is the Keplerian part of the system, where  $\mathcal{G}$  is the gravitational constant and  $\mathcal{H}_R = T_R$  is referred as the Euler system (or the free rigid body). More explicitly, we obtain the following expression for  $\mathcal{H}$  in the  $\mathcal{B}_1$ -body frame

$$\mathcal{H}(\mathbf{r}, \mathbf{A}, \mathbf{p}, \mathbf{\Pi}) = \frac{|\mathbf{p}|^2}{2m} + \frac{1}{2} \mathbf{\Pi} \cdot \mathbf{I}^{-1} \cdot \mathbf{\Pi} - \mathcal{G} m_2 \int_{\mathcal{B}_1} \frac{dm_1(\mathbf{x}_1)}{|\mathbf{r} - \mathbf{x}_1|}, \quad (2)$$

where  $m = m_1 m_2 / (m_1 + m_2)$ ,  $\mathbf{r}$  is the vector joining the center of mass of the bodies,  $\mathbf{A}$  is the rotation matrix transforming a vector in the body-fixed frame into the inertial frame and  $\mathbf{p}$  and  $\mathbf{\Pi}$  are the linear and angular momenta. In addition, the assumption (iii) allows us to consider the approximation of the gravitational potential  $\mathcal{P}$  given by  $-\mathcal{G}M/r$  and the MacCullagh's term [26]

$$U = -\frac{\kappa m}{2m_1 r^3} [(A_3 - A_2)(1 - 3\gamma_3^2) - (A_2 - A_1)(1 - 3\gamma_1^2)], \quad (3)$$

where  $\kappa = \mathcal{G}M$ ,  $M = m_1 + m_2$  is the total mass of the system,  $A_1 \leq A_2 \leq A_3$  are the principal moments of inertia associated to the secondary body and  $(\gamma_1, \gamma_2, \gamma_3)$  are the director cosines of  $\mathbf{r}$ .

## 2.1 MacCullagh's term in variables referred to the total angular momentum

The variables in which the problem is posed may have a significant impact on its treatment. Our choice is the use of the total angular momentum as the key object to define them, which application for the roto-translatory problem was first introduced in [17] as a result of the application of the elimination of the nodes in the  $n$ -body problem [15] to the roto-translatory model. Nevertheless, there is a saying in celestial mechanics that no set of coordinates is good enough. This claim highlights that in every choice of variables, a sacrifice must be done. More precisely, Cartesian variables have a simple formulation, but they do not take advantage of the presence of symmetries. Conversely, by using variables referred to the total angular momentum, we incorporate the angles associated to the symmetries allowing for compact expressions and intuitive geometric insight of the relative equilibria. However, this is done at the expenses of having singularities, *i. e.* a global study of the system requires the use of several charts.

The complete set of canonical variables is  $(r, \phi, \psi, \theta, \delta, \nu, R, \Phi, \Psi, \Theta, \Delta, N)$ . We are not going to provide a complete derivation of them, which may be found in [17, 23]. Instead and with the aim of fixing notation, we provide the geometric meaning of the angles by means of Figure 1 and briefly recall the definition of the canonical angles by following [11]: Let us consider the reference frame  $S^* = (\ell, \mathbf{n} \times \ell, \mathbf{n})$ , where  $\ell$  is the unitary vector defining node of the total angular momentum plane with the horizontal spatial plane and  $\mathbf{n}$  is the unitary vector pointing in the direction of the total angular momentum. In addition,  $S^E = \{\mathbf{E}_1, \mathbf{E}_2, \mathbf{E}_3\}$  and  $S^b = \{\mathbf{b}_1, \mathbf{b}_2, \mathbf{b}_3\}$  are the spatial and body frames respectively, where  $\mathbf{b}_i$  corresponds with the principal moment of inertia of  $\mathcal{B}_1$ . The orientation and center of mass of the body are referred to the new frame by means of  $(r, \phi, \psi, \theta, \delta, \nu)$ , see Figure 1. These angles are determined by the nodes;  $\ell_{\mu\delta}$  defined by the rotational angular momentum and the spatial plane,  $\ell_r = -\ell_o$  given by the intersection of the total, rotational and orbital angular momentum planes and  $\ell_\theta$  generated by the orbital and spatial planes intersection. Precisely, we have that  $\phi = (\widehat{\mathbf{E}_1, \ell})$ ,  $\psi = (\widehat{\ell, \ell_I})$ ,  $\theta = (\widehat{\ell_o, \mathbf{r}})$ ,  $\delta = (\widehat{\ell_r, \ell_I})$  and  $\nu = (\widehat{\ell_I, \mathbf{b}_1})$ . Moreover, there are three more auxiliary angles which are not among the canonical variables but we will use them later on;  $\lambda = (\widehat{\mathbf{E}_1, \ell})$ ,  $\mu = (\widehat{\ell_{\mu\delta}, \ell_I})$ ,  $\sigma = (\widehat{\Pi_r, \Pi_b})$  and  $h = (\widehat{\mathbf{E}_1, \ell_\theta})$ .

In addition, the conjugate momenta of the variables read as follows

$$R, \quad \Phi = \mathbf{G} \cdot \mathbf{E}_3, \quad \Psi = \mathbf{G} \cdot \mathbf{n} = G, \quad \Theta = G_o, \quad \Delta = G_r, \quad N = \mathbf{G}_r \cdot \mathbf{b}_3, \quad (4)$$

where  $\mathbf{G}$  is the total angular momentum vector,  $\mathbf{G}_r$  is the angular momentum of the secondary body in the body frame and  $\mathbf{G}_o$  is the orbital angular momentum. Thus, we have the following interpretation of the momenta: ( $R$ ) Radial velocity of the center of mass. ( $\Phi$ ) Third component of the total angular momentum in space frame. ( $\Psi$ ) Magnitude of the total angular momentum. ( $\Theta$ ) Magnitude of the angular momentum of the center of mass. ( $\Delta$ ) Magnitude of the angular momentum of the rigid body. ( $N$ ) Third component of the angular momentum of the rigid body in the body frame (principal axes of inertia).

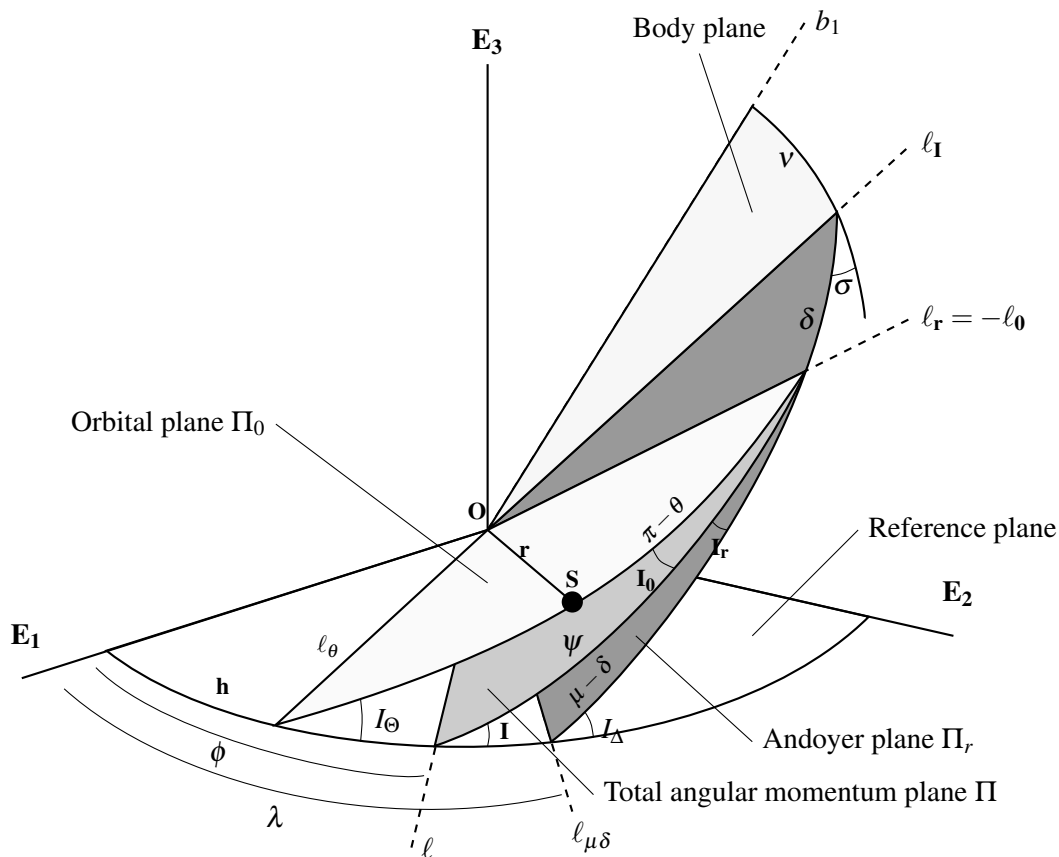


**Fig. 1** Geometry of the variables ( $r, \phi, \psi, \theta, \delta, v, R, \Phi, \Psi, \Theta, \Delta, N$ ). The variable  $r$  and the angles are explicitly given in the figure, while the associated momenta are included implicitly through the inclinations of the planes. The conjugate variable  $R$  remains unrepresented because of its pure dynamical sense.

Finally, we gather below the formulas for the relative positions of the different planes, as functions of the canonical momenta, which are given by

$$\cos(I_o + I_r) = \frac{\Psi^2 - \Delta^2 - \Theta^2}{2\Theta\Delta}, \quad \cos I_r = \frac{\Psi^2 + \Delta^2 - \Theta^2}{2\Psi\Delta}, \quad (5)$$

$$\cos I_o = \frac{\Psi^2 + \Theta^2 - \Delta^2}{2\Psi\Theta}, \quad \cos \sigma = \frac{N}{\Delta}, \quad \cos I = \frac{\Phi}{\Psi} \quad (6)$$

and the following relations between angles and momenta hold

$$\Psi = \Delta \cos I_r + \Theta \cos I_o, \quad \frac{\Delta}{\sin I_o} = \frac{\Theta}{\sin I_r} = \frac{\Psi}{\sin(t)}, \quad (7)$$

where  $I$  is the inclination of the total angular momentum plane  $\Pi$ ,  $I_o$  and  $I_r$  are the inclinations of the orbital and rotational planes with respect to  $\Pi$  and  $\iota = I_o + I_r$ .

The direction cosines appearing in (3) may be expressed in the body frame by means of the following composition of rotations:

$$\gamma = R_3(\nu) R_1(\sigma) R_3(\delta) R_1(\iota) R_3(\pi - \theta) \mathbf{e}_1 \quad (8)$$

where  $\gamma = (\gamma_1, \gamma_2, \gamma_3)$  and  $\mathbf{e}_1 = (1, 0, 0)$ . Finally, taking into account that  $\gamma_1^2 + \gamma_2^2 + \gamma_3^2 = 1$  and after some calculations, we are allowed to express the MacCullagh's term (3) as follows

$$U = \frac{km}{32m_1r^3} \left[ (2A_3 - A_2 - A_1)V_1 + \frac{3}{2}(A_2 - A_1)V_2 \right], \quad (9)$$

where

$$\begin{aligned} V_1 = & -2(1 - 3c_t^2)(1 - 3c_\sigma^2) \\ & - 3s_\sigma^2 \left[ (1 - c_t)^2 C_{2,2,0} + (1 + c_t)^2 C_{-2,2,0} \right] \\ & - 6s_t^2 \left[ s_\sigma^2 C_{0,2,0} - (1 - 3c_\sigma^2) C_{2,0,0} \right] \\ & + 12c_\sigma s_t s_\sigma \left[ (1 - c_t) C_{2,1,0} + 2c_t C_{0,1,0} - (1 + c_t) C_{-2,1,0} \right] \end{aligned} \quad (10)$$

which is independent of  $\nu$ , and  $V_2$ , the ‘‘triaxiality part’’ given by

$$\begin{aligned} V_2 = & -(1 - c_\sigma)^2 \left[ (1 - c_t)^2 C_{2,2,-2} + (1 + c_t)^2 C_{-2,2,-2} + 2s_t^2 C_{0,2,-2} \right] \\ & - (1 + c_\sigma)^2 \left[ (1 - c_t)^2 C_{2,2,2} + (1 + c_t)^2 C_{-2,2,2} + 2s_t^2 C_{0,2,2} \right] \\ & - 6s_t^2 s_\sigma^2 \left[ C_{2,0,2} + C_{2,0,-2} \right] + 4s_\sigma^2 (1 - 3c_t^2) C_{0,0,2} \\ & + 4s_t s_\sigma (1 - c_\sigma) \left[ (1 - c_t) C_{2,1,-2} + 2c_t C_{0,1,-2} - (1 + c_t) C_{-2,1,-2} \right] \\ & + 4s_t s_\sigma (1 + c_\sigma) \left[ -(1 - c_t) C_{2,1,2} - 2c_t C_{0,1,2} + (1 + c_t) C_{-2,1,2} \right], \end{aligned} \quad (11)$$

and the notation has been abbreviated by writing  $C_{i,j,k} \equiv \cos(i\theta + j\delta + kv)$  and  $c_x \equiv \cos x$  and  $s_x \equiv \sin x$ .

## 2.2 Intermediary model

Facing a non-integrable Hamiltonian system requires the development of a perturbation theory. A usual way to proceed is to expand the Hamiltonian function in power series and truncate it at a certain order. This procedure is in general an uncontrolled approximation since, for most cases, we are no longer sure that the solutions of the truncated model stay close to the full model. In the case of the FG2BP, it is customary to consider the orbital and rotational kinetic energies and choose the first term in the expansion of the gravitational potential, see (1). Thus, we end up with the free rigid body Hamiltonian (the rotational kinetic energy) and the Kepler system Hamiltonian. That is, the orbital kinetic energy plus the first non-zero term of the gravitational potential. However, there is no any theorem claiming that this is the only way it can be done. The novelty of an intermediary model is that it allows to consider truncation of partial order in the power series expansion. In other words, we pick some ‘‘entire’’ terms of the power series plus a ‘‘piece’’ of one term. The only requirement that must be fulfilled in this procedure is that the intermediary model should be searchable.

In [11], the authors proposed an axis-symmetric integrable intermediary model, whose accuracy was tested by comparing with the MacCullagh's truncation and showing a good performance in the numerical experiments. Here, we complete this previous study by investigating the triaxial case. One of our aims is to analyze the physical-parametric bifurcations of relative equilibria due to the elimination of the axial symmetry of the body. Keeping this motivation in mind, we propose our intermediary following exactly the same procedure than in [11],

except for the triaxial parameter. That is to say, we only take into account the first line of  $V_1$  in (10). Then, let the perturbing potential of the intermediary model be given by

$$\mathcal{V} = -\frac{km}{16m_1r^3}(2A_3 - A_2 - A_1)(1 - 3c_i^2)(1 - 3c_\sigma^2), \tag{12}$$

which leads us to the final expression of the intermediary Hamiltonian

$$\begin{aligned} \mathcal{H} = & \frac{1}{2} \left( R^2 + \frac{\Theta^2}{r^2} \right) - \frac{\kappa}{r} + \frac{q}{2} \left[ \left( \frac{\sin^2(\nu)}{A_1} + \frac{\cos^2(\nu)}{A_2} \right) (\Delta^2 - N^2) + \frac{1}{C} N^2 \right] \\ & - \frac{\kappa(2A_3 - A_2 - A_1)}{16r^3} (1 - 3c_i^2) (1 - 3c_\sigma^2), \end{aligned} \tag{13}$$

where  $q = m/m_1$ . Furthermore, with the aim of alleviate formulas, we have considered the Hamiltonian per unit of mass by scaling the system and inertia momenta as follows:

$$\begin{aligned} \mathcal{H}' = \mathcal{H}/m; \quad R' = R/m; \quad \Theta' = \Theta/m; \quad \Delta' = \Delta/m; \quad N' = N/m; \quad \Psi' = \Psi/m; \\ \Phi' = \Phi/m; \quad A'_1 = A_1/m_1; \quad A'_2 = A_2/m_1; \quad A'_3 = A_3/m_1. \end{aligned} \tag{14}$$

Nevertheless, for the sake of simplicity, we keep the original notation without primes on the variables. Then, the 2-DOF Hamiltonian system of differential equations associated with (13) is given by the following expressions:

$$\dot{r} = R \tag{15}$$

$$\dot{R} = \frac{\Theta^2}{r^3} - \kappa \frac{1}{r^2} - \frac{3\alpha\kappa}{16r^4} (1 - 3c_i^2) (1 - 3c_\sigma^2) \tag{16}$$

$$\dot{\theta} = \frac{\Theta}{r^2} - \frac{3\alpha\kappa}{8\Theta r^3} c_i (1 - 3c_\sigma^2) \left( c_i + \frac{\Theta}{\Delta} \right) \tag{17}$$

$$\dot{\psi} = \frac{3\alpha\kappa\Psi}{8\Delta\Theta r^3} c_i (1 - 3c_\sigma^2) \tag{18}$$

$$\dot{\delta} = \left[ q \left( \frac{\sin^2(\nu)}{A_1} + \frac{\cos^2(\nu)}{A_2} \right) - \frac{3\alpha\kappa}{8\Delta^2 r^3} \left( (1 - 3c_i^2) c_\sigma^2 + c_i (1 - 3c_\sigma^2) \left( c_i + \frac{\Delta}{\Theta} \right) \right) \right] \Delta \tag{19}$$

$$\dot{\nu} = \left[ \frac{q}{A_3} - q \left( \frac{\sin^2(\nu)}{A_1} + \frac{\cos^2(\nu)}{A_2} \right) + \frac{3\alpha\kappa}{8\Delta^2 r^3} (1 - 3c_i^2) \right] N \tag{20}$$

$$\dot{N} = q \frac{(A_1 - A_2)}{2A_1A_2} (\Delta^2 - N^2) \sin(2\nu) \tag{21}$$

together with the integrals  $\dot{\Theta} = \dot{\phi} = \dot{\Phi} = \dot{\Psi} = \dot{\Delta} = 0$ .

Note that, in general, a 2-DOF system is not integrable. Thus, in the triaxial case, the analytical integration is not provided and the integrability of the system remains as an open question, which is not in the scope of the present paper.

### 3 Numerical experiments

In this section we present numerical experiment comparing the intermediary versus the full model (MacCullagh’s approximation). For this purpose, we sweep three parameters that allow us to define the usability of the triaxial intermediary model. In the first scenario, we recover the triaxiality parameter  $\rho$  defined in [10], which is given by the following expression

$$\rho = \frac{A_2 - A_1}{2A_3 - A_2 - A_1}, \tag{22}$$

and allows us to assess the impact of the triaxiality in the performance of the model. Next, we analyze the role of the eccentricity and height (distance between the bodies surfaces) by carrying out simulations with these parameters ranging from  $e \in [0, 0.5]$  and height between 1000 and 2000 km.

Before we get into the numerical evaluations, it is important to pay some attention to the way in which we proceeded. With the aim of keeping track of the geometry, the initial conditions for the variables are not given directly. Namely, we introduce some of the canonical momenta by means of the set  $(e, \mu, \sigma, I_o, I_r, I)$ , where  $e$  is the initial eccentricity of the trajectory. For the readers interested in performing their own experiments, we include in the Appendix the formulas allowing to connect the previous set with the corresponding canonical variables. That is to say, in our simulations we set  $(r_0, \phi_0, \psi_0, \theta_0, \sigma_0, v_0, e, \mu_0, R_0, I_o, I_r, I)$  and then we obtain the corresponding initial canonical variables  $(r_0, \phi_0, \psi_0, \theta_0, \delta_0, v_0, R_0, \Phi_0, \Psi_0, \Theta_0, \Delta_0, N_0)$ .

Additionally, in order to reproduce the numerical experiment, it is very important to keep in mind throughout this section that we have introduced some simplifications. Namely, we have considered the Hamiltonian per unit of mass and the canonical and inertia momenta have been scaled, see (14). Furthermore, we have changed internally the units for longitudes by choosing the new one as the radius of the spherical body  $R_p$ . However, we set these units back to Km when we present our results. Regarding to the initial conditions, the radius and angles (radians) are given directly. The following experiments are carried out for fixed values of the initial conditions and parameters with the exception of the eccentricity, height and principal moments of inertia, which will be specified for each simulation. We consider the scenario of a massive spheric primary and an arbitrary secondary. More precisely, the two bodies are given by; Main body  $\mathcal{B}_2$ : a sphere with radius 500 Km and mean density  $d = 2.8 \text{ g/cm}^3$ , then mass is given by  $m_2 = 1.47 \cdot 10^{21} \text{ Kg}$ . Body  $\mathcal{B}_1$ : an ellipsoid with mean density  $d = 1.4 \text{ g/cm}^3$ , the principal axes will be given for each simulation. Solutions are evaluated for one orbital period.

### 3.1 Parameter analyzed: Triaxiality

In this part we analyze the impact of the triaxiality parameter  $\rho$ . For this purpose we fix eccentricity to zero in all the evaluations and consider four different triaxialities by modifying the secondary body principal axes. Precisely we study the cases  $\rho \in \{0, 0.0005, 0.15, 0.35\}$ , which measure the evolution of the model when  $\rho$  ranges from the axial-symmetric case to a moderate triaxiality. In Figure 3 it is shown how the performance becomes poorer as the triaxiality parameter grows. More in detail, we observe for the radial variable that differences duplicate in each step from  $\rho = 0$  to  $\rho = 0.35$ . Analogously, slow angles  $\psi$  and  $\theta$  reduce their accuracy. However, in this case there is a drastic change from the axial-symmetric case to the first step into the triaxial model, which increases differences by a factor of ten. Moreover, there is also a significant difference in the behavior of these angles, since the differences with the full model are now strict monotone functions instead of having an oscillatory nature as in the axial-symmetric case. Rather than the expected and moderate degradation in performance of the radial and the slow-angles, the main novelty in the triaxial case with respect to the axial symmetric one is that their approximation deteriorates more and much faster. For that reason and for the sake of brevity, fast angles will not be displayed in the following sections, since their behavior is quite similar.

Before we present our experiments in the general case, we study in detail the transition from  $\rho = 0$  to a very low triaxiality. In this regard, Figure 2 shows how fast angles behaves for a nearly zero triaxiality. It is observed that the announced degradation in accuracy depends gradually on the triaxiality parameter  $\rho$ , though it is presented very early. However, our experiments are given for fast rotating bodies. As such, an analysis for the case of slow rotating bodies is required in order to find out how the rotational angular momentum modulus influences in accuracy.

Now we consider the case of higher triaxialities. Despite of what have been said, these experiments still show a very high accuracy for moderate values of  $\rho$ . Namely, in all the simulations provided in Figure 3, the error ratio  $(r_{Interm} - r_{full})/r_0$  is under 0.00064% after one orbital period and for the slow angles we obtain differences up to the order  $10^{-6}$  radians. Fast angles are no longer well approximated.

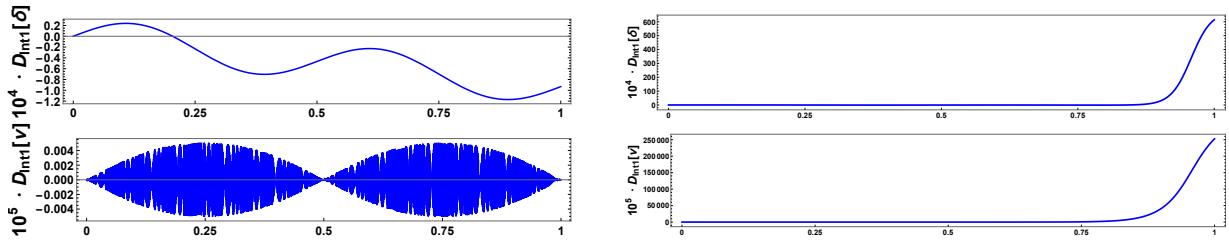


**Fig. 2** Columns from left to right we have: (i)  $\rho = 0$ ,  $A_1 = 9.80 \cdot 10^{20}$ ,  $A_2 = 9.8 \cdot 10^{20}$ ,  $A_3 = 1.07 \cdot 10^{21}$ . (ii)  $\rho = 0.0005$ ,  $A_1 = 1.17 \cdot 10^{21}$ ,  $A_2 = 1.23 \cdot 10^{21}$ ,  $A_3 = 1.39 \cdot 10^{21}$ . Abscissas are orbital periods and  $D[x] = x_{Full} - x_{Intermediary}$ . The orbital period is 10.8 hours and  $r$  is expressed in Km, which initially is set to 1.560 Km.

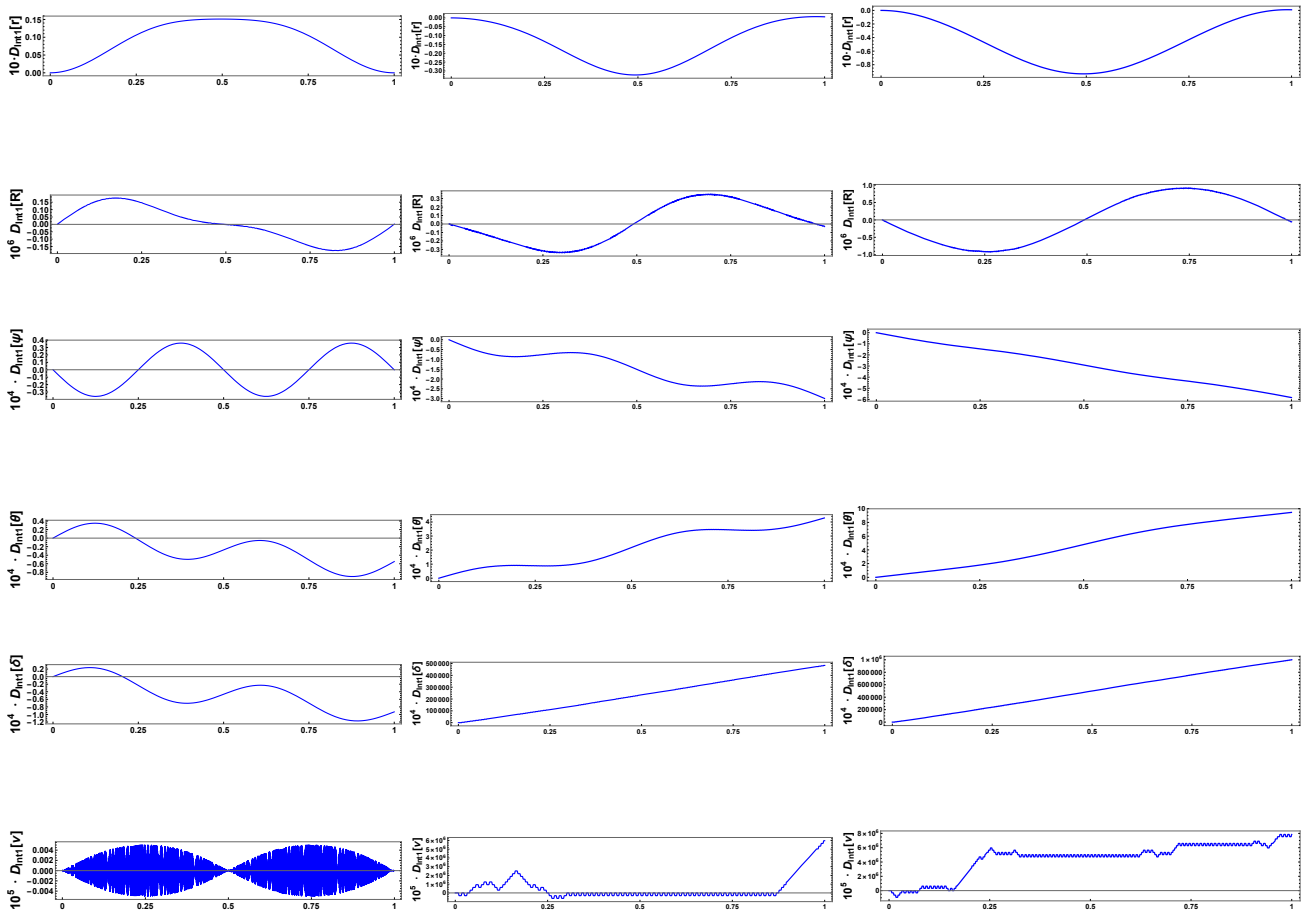


**Fig. 3** Columns from left to right we have: (i)  $\rho = 0$ ,  $A_1 = 9.80 \cdot 10^{20}$ ,  $A_2 = 9.8 \cdot 10^{20}$ ,  $A_3 = 1.07 \cdot 10^{21}$ . (ii)  $\rho = 0.15$ ,  $A_1 = 1.17 \cdot 10^{21}$ ,  $A_2 = 1.23 \cdot 10^{21}$ ,  $A_3 = 1.39 \cdot 10^{21}$ . (iii)  $\rho = 0.35$ ,  $A_1 = 1.06 \cdot 10^{21}$ ,  $A_2 = 1.18 \cdot 10^{21}$ ,  $A_3 = 1.28 \cdot 10^{21}$ . Abscissas are orbital periods and  $D[x] = x_{Full} - x_{Intermediary}$ . The orbital period is 10.8 hours and  $r$  is expressed in Km, which initially is set to 1.560 Km.

Initial conditions for simulations in Figure 2 and Figure 3.

$$\begin{aligned}
 r_0 &= 1550, \phi_0 = \frac{2\pi}{9}, \psi_0 = \frac{\pi}{4}, \theta_0 = 0, \sigma_0 = \frac{\pi}{2}, v_0 = 0, \\
 \mu_0 &= \frac{7\pi}{18}, R_0 = 0, I_o = \frac{\pi}{18}, I_r = \frac{\pi}{12}, I = \frac{7\pi}{36}, e = 0,
 \end{aligned}
 \tag{23}$$

making use of the formulas in the Appendix, we are led to the following initial values for the canonical variables

$$\begin{aligned} r_0 = 3.12 \cdot R_p, \quad \phi_0 = 0.698131, \quad \psi_0 = 0.785398, \quad \theta_0 = 0, \quad \delta_0 = 0.630221, \quad v_0 = 0, \\ R_0 = 0, \quad \Phi_0 = 0.125460, \quad \Psi_0 = 0.153158, \quad \Theta_0 = 0.093797, \quad \Delta_0 = 0.062930, \quad N_0 = 0. \end{aligned} \quad (24)$$

### 3.2 Parameter analyzed: Eccentricity

In the formulation of the triaxial model in Section 2 we restrict the validity of the model to small eccentricities. That is to say, we consider eccentricity up to 0.5, since for higher values even the full model (MacCullagh's approximation) does not provide a valuable estimation. In Figure 4  $e$  is set to 0.1 and 0.5, showing that accuracy decreases by factor two as eccentricity grows and leading to a similar scenario than in the triaxiality analysis.

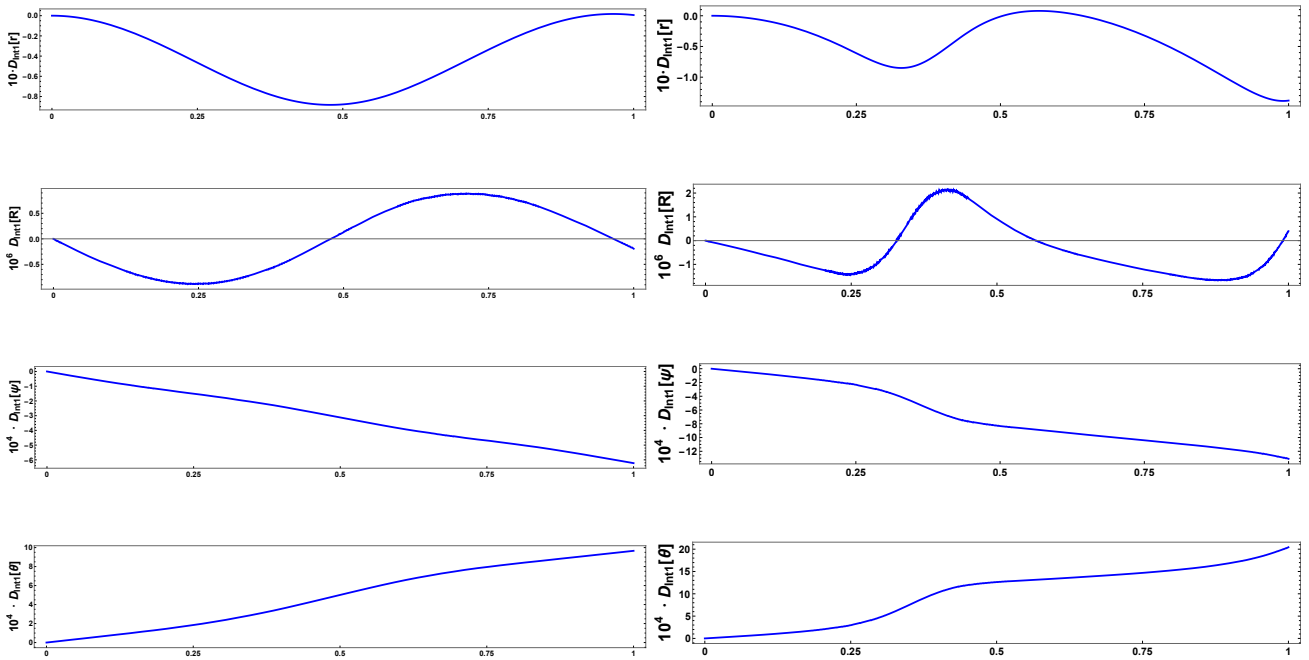


**Fig. 4** Left column  $e = 0.1$  and right column  $e = 0.5$ . Abscissas are orbital periods and  $D[x] = x_{Full} - x_{Intermediary}$ . The orbital period is 10.8 hours and  $r$  is expressed in Km, which initially is set to 1.560 Km.

Next, we specify the initial conditions and parameters to assess the role of the eccentricity. Firstly, we fix the dimensions of the secondary body to be 60, 55 and 45 Km. Then, we obtain the following associated moments of inertia

$$A_1 = 1.06 \cdot 10^{21}, \quad A_2 = 1.18 \cdot 10^{21}, \quad A_3 = 1.28 \cdot 10^{21}.$$

The remaining variables, inclinations and momenta are also fixed with the exception of the eccentricity

$$\begin{aligned} r_0 = 1550, \quad \phi_0 = \frac{2\pi}{9}, \quad \psi_0 = \frac{\pi}{4}, \quad \theta_0 = 0, \quad \sigma_0 = \frac{\pi}{2}, \quad v_0 = 0, \\ \mu_0 = \frac{7\pi}{18}, \quad R_0 = 0, \quad I_o = \frac{\pi}{18}, \quad I_r = \frac{\pi}{12}, \quad I = \frac{7\pi}{36}, \quad e, \end{aligned} \quad (25)$$

making use of the formulas in the Appendix, we are led to the corresponding initial values for each value of the

eccentricity. Namely, for  $e = 0.1$  we obtain

$$\begin{aligned} r_0 = 3.12 \cdot R_p, \quad \phi_0 = 0.698131, \quad \psi_0 = 0.785398, \quad \theta_0 = 0, \quad \delta_0 = 0.630221, \quad v_0 = 0, \\ R_0 = 0, \quad \Phi_0 = 0.124829, \quad \Psi_0 = 0.152388, \quad \Theta_0 = 0.09332, \quad \Delta_0 = 0.062614, \quad N_0 = 0, \end{aligned} \tag{26}$$

and for  $e = 0.5$

$$\begin{aligned} r_0 = 3.12 \cdot R_p, \quad \phi_0 = 0.698131, \quad \psi_0 = 0.785398, \quad \theta_0 = 0, \quad \delta_0 = 0.630221, \quad v_0 = 0, \\ R_0 = 0, \quad \Phi_0 = 0.108650, \quad \Psi_0 = 0.132637, \quad \Theta_0 = 0.081229, \quad \Delta_0 = 0.054498, \quad N_0 = 0. \end{aligned} \tag{27}$$

### 3.3 Parameter analyzed: Height

This section present a representative selection for a low range of altitudes. In Figure 5 we compare the results obtained for 1000 and 2000 Km, with fixed  $e = 0.3$ , showing that a different picture emerges for the height analysis. Namely, accuracy is enhanced, at least duplicated, with height. However, a more exhaustive study considering a wider range of altitudes should be done to clarify at what extend is this claim true.

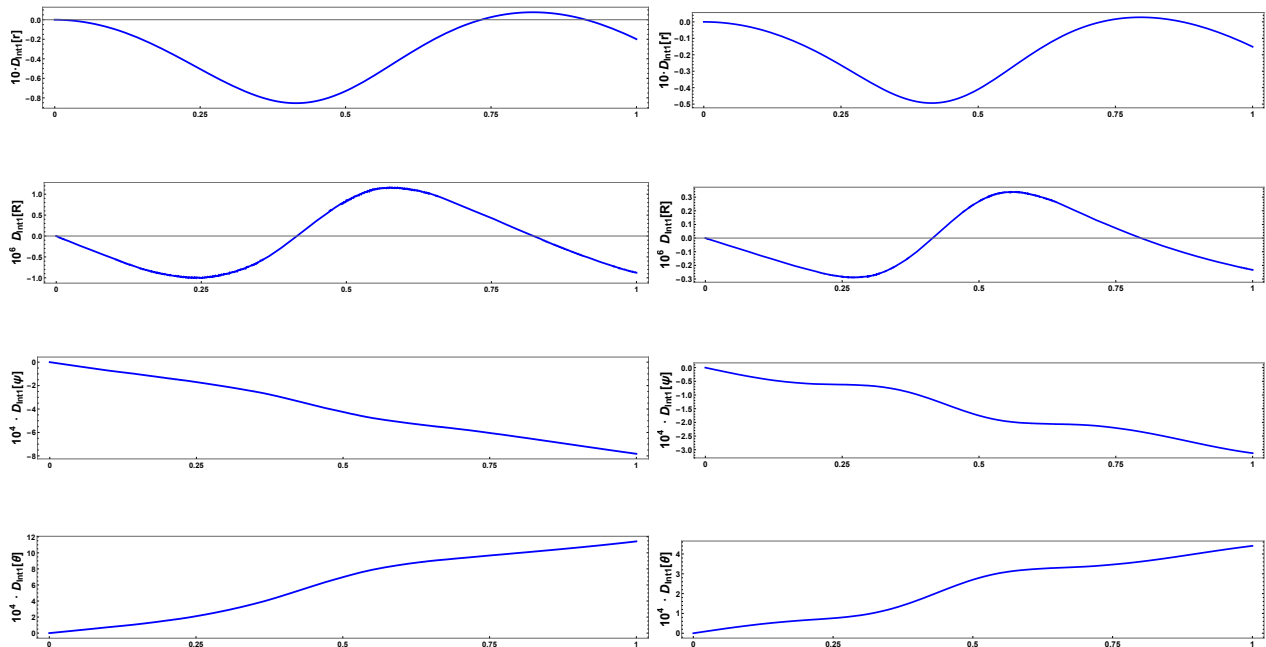


**Fig. 5** Left column ( $H = 1000\text{ Km}, T = 22.8\text{ h}$ ) and right column ( $H = 2000\text{ Km}, T = 10.8\text{ h}$ ), where  $T$  is the orbital period expressed in hours. Abscissas are orbital periods and  $D[x] = x_{Full} - x_{Intermediary}$

Initial conditions and parameters are set as follows

$$\begin{aligned} r_0 = 1550, \quad \phi_0 = \frac{2\pi}{9}, \quad \psi_0 = \frac{\pi}{4}, \quad \theta_0 = 0, \quad \sigma_0 = \frac{\pi}{2}, \quad v_0 = 0, \\ \mu_0 = \frac{7\pi}{18}, \quad R_0 = 0, \quad I_o = \frac{\pi}{18}, \quad I_r = \frac{\pi}{12}, \quad I = \frac{7\pi}{36}, \quad e = 0.3, \end{aligned} \tag{28}$$

Then, we obtain the following initial conditions for heights  $H = 1000$  and  $H = 2000$  Km accordingly

$$\begin{aligned} r_0 = 3.12 \cdot R_p, \quad \phi_0 = 0.698131, \quad \psi_0 = 0.785398, \quad \theta_0 = 0, \quad \delta_0 = 0.630221, \quad v_0 = 0, \\ R_0 = 0, \quad \Phi_0 = 0.119679, \quad \Psi_0 = 0.146101, \quad \Theta_0 = 0.0894754, \quad \Delta_0 = 0.060031, \quad N_0 = 0, \end{aligned} \tag{29}$$

for height=1000Km and

$$\begin{aligned} r_0 = 5.12 \cdot R_p, \quad \phi_0 = 0.698131, \quad \psi_0 = 0.187160, \quad \theta_0 = 0, \quad \delta_0 = 0.630221, \quad v_0 = 0, \\ R_0 = 0, \quad \Phi_0 = 0.153312, \quad \Psi_0 = 0.146101, \quad \Theta_0 = 0.114620, \quad \Delta_0 = 0.076901, \quad N_0 = 0, \end{aligned} \quad (30)$$

for height=2000Km.

#### 4 Searching for relative equilibria. Constant radius solutions

The system of differential equations defined by the Hamiltonian (13) is endowed with several distinguish and physical parameters. Thus, bifurcations occurs in several directions in the parametric space. With the aim of simplifying this scenario and provide a clear geometric interpretation of our equilibria, we organize our families of relative equilibria according to the inclinations of pairs of fundamental planes (orbital, rotational and body planes). More precisely, we consider the relative inclination between orbital and rotational planes ( $\iota$ ) and the one determined by the rotational and body planes ( $\sigma$ ). For that reason  $\cos \iota$  and  $\cos \sigma$  are the key objects to present the analysis of the relative equilibria. Precisely, we show that  $\cos \iota = \pm\sqrt{1/3}$  allows for the appearance of the families dubbed as critical inclination equilibria. Apart from that, from the angle between the body and rotational planes we obtain body-inclined equilibria ( $\cos \sigma \neq 0$ ) and body-perpendicular equilibria ( $\cos \sigma = 0$ ). Note that the nomenclature of the families of equilibria related to the angle  $\sigma$  has been prefixed with the word *body*. It is done with the aim of distinguishing these equilibria from those dubbed as inclined and perpendicular equilibria in [10], which are related to the dihedral angle  $\iota$ .

However, the physical parameters do also give rise to bifurcations. Namely, the number and nature of equilibria depends on the moments of inertia ( $A_1, A_2, A_3$ ), which for the axis-symmetric case leads to extra families of equilibria studied in [11]. Additionally, in [10], we also identify a special triaxiality for  $\rho = 1/3$  leading to a family of equilibria. However, the triaxial parameter  $\rho$  does not play the same role in the present intermediary. This fact is due to the elimination of the contribution of  $V_2$  in our model, which makes the triaxiality hinges in  $\alpha = (2A_3 - A_2 - A_1)$ .

We begin our study by looking for a possible relative equilibrium of our Hamiltonian system with constant radius, which leads to solutions living in a 4-D torus. Then, we proceed with the study of conditions leading to lower dimensional tori. We would like to remark that we are not going to carry out an exhaustive study of all the equilibria of this intermediary, since it would require the use of variables free of singularities which is beyond the scope of this paper and it is a research in progress part of [6]. Henceforth, we consider the following notation

$$v_i = i\frac{\pi}{2}, \quad i \in \{1, 2, 3, 4\}. \quad (31)$$

Observe that on one hand, the cases  $\{v_1, v_3\}$  lead us to the presence of  $A_1$  in the formulas (19) and (20) and on the other hand cases  $\{v_2, v_4\}$  lead us to the presence of  $A_2$  respectively.

##### 4.1 Critical inclination equilibria

Along this subsection we study the equilibria obtained under a fixed inclination of the dihedral angle  $\iota$  which determines the relative position of the orbital and rotational planes. In particular we consider  $(1 - 3c_1^2) = 0$ , i.e.  $c_1 = \pm\sqrt{1/3}$ , inclination dubbed as critical inclination. Observe that for this critical inclination the perturbative term in (16) and (20) vanishes and these two equations correspond with the decoupled motion of the Kepler and the free rigid body problems respectively.

- *Invariant 4-tori*  $\mathbb{T}^4(\theta, \psi, \delta, v)$ .

Our first approach to tackle the problem of searching for orbits of constant radius within our intermediary is by examining the subsystem  $(\dot{r}, \dot{R})$ , i.e. equations (15) and (16). Just by being  $(1 - 3c_1^2) = 0$  we get an

equilibrium of  $(\dot{r}, \dot{R})$  which provide us the following expression for the constant radius:

$$r = \frac{\Theta^2}{\kappa}. \quad (32)$$

The orbits obtained under this inclination are restricted to be into the invariant  $\mathbb{T}^4(\theta, \psi, \delta, \nu)$ .

## 4.2 Body-Inclined equilibria

Following the classification previously indicated, we study here the equilibria obtained under a fixed inclination of the  $\sigma$  angle. In particular, we called inclined equilibria to those for which  $c_\sigma \neq 0$ , i.e.  $N \neq 0$ . Due to the factorization obtained of (20) and in order to obtain orbits of constant radius for this family of equilibria we have:

$$\frac{q}{A_3} - \frac{q}{A_i} + \frac{3\alpha\kappa}{8} \frac{(1 - 3c_i^2)}{\Delta^2 r^3} = 0, \quad i \in \{1, 2\}. \quad (33)$$

Note that the above formula implies  $(1 - 3c_i^2) > 0$  and the following restriction for  $\Delta$

$$\Delta^2 \leq \frac{3\alpha\kappa}{8qr^3} \left( \frac{A_3 A_i}{A_3 - A_i} \right). \quad (34)$$

As result of the appearance of the  $r$  cubed constrain in the denominator we have that these equilibria are just possible for very small values of  $\Delta$ , which implies bodies in a slow rotational regime.

- *Fixed  $\nu$ . Invariant 3-tori  $\mathbb{T}^3(\theta, \psi, \delta)$ .*

Considering the subsystems  $(\dot{r}, \dot{R})$  and  $(\dot{\nu}, \dot{N})$  under a inclined equilibria and  $1 - 3c_\sigma^2 \neq 0$  along with some particular initial value problem conditions, i.e.  $R = 0$ ,  $\nu = \nu_i$ ,  $N \neq 0$ ,  $1 - 3c_\sigma^2 \neq 0$ , from (16) and (20) we obtain an expression for the radius

$$r = \frac{\Theta^2}{2\kappa} + \sqrt{\frac{\Theta^4}{4\kappa^2} - \frac{3\alpha(1 - 3c_i^2)(1 - 3c_\sigma^2)}{16}}, \quad (35)$$

which leads to an implicit relation between  $c_i$  and  $c_\sigma$  which provides us equilibrium that guarantees us the existence of orbits of constant radius within the invariant 3-tori  $\mathbb{T}^3(\theta, \psi, \delta)$

$$\sqrt[3]{\frac{3\alpha\kappa(1 - 3c_i^2)A_i A_3}{8\Delta^2 q(A_3 - A_i)}} = \sqrt{\frac{\Theta^4}{4\kappa^2} - \frac{3}{16}\alpha(1 - 3c_i^2)(1 - 3c_\sigma^2)} + \frac{\Theta^2}{2\kappa}. \quad (36)$$

Using Taylor series of the previous expression of  $c_i$  about 0 we obtain the zero order approximation of  $c_\sigma$

$$c_\sigma = -\frac{\sqrt{16a\Theta^2 + 16a^2\kappa + 3\alpha\kappa}}{3\sqrt{\alpha\kappa}},$$

where

$$a = \sqrt[3]{\frac{3\alpha A_1 A_3 \kappa}{8\Delta^2 q(A_1 - A_3)}}.$$

This expression shows us how the triaxiality of  $B_1$  connects the relation between  $c_\sigma$  and  $c_i$ .

Searching for conditions that lead us to find equilibria for  $\delta$  and  $\psi$  within our 3-tori we notice analyzing (18) and (19) that there is no a simultaneous equilibrium for  $\delta$  and  $\psi$ . Therefore, we continue studying the existence of 2-tori originated by fixing one of the remaining angles.

- *Fixed  $v$  and  $\delta$ . Invariant 2-tori  $\mathbb{T}^2(\theta, \psi)$*

We examine now the subsystem  $(\dot{\delta}, \dot{\Delta})$  under the same inclination and initial value problem established previously. Taking into account (19) we get a fixed inclination that allows us to find an equilibrium of  $\delta$  within our 3-tori and consequently we find particular body-inclined equilibria that guarantee us the existence of orbits within the invariant 2-tori  $\mathbb{T}^2(\theta, \psi)$ .

The variation of the remainder angles for these orbits are:

$$\dot{\theta} = n_{\theta} = \frac{\Theta}{r^2} - \frac{3\alpha\kappa c_l(1-3c_l^2)(c_l + \frac{\Theta}{\Delta})}{8\Theta r^3}, \quad (37)$$

$$\dot{\psi} = n_{\psi} = \frac{3\alpha\kappa c_l(1-3c_l^2)\Psi}{8\Delta\Theta r^3}. \quad (38)$$

Under this particular body-inclined equilibria the relations between inclinations are given by:

$$c_{\sigma_1}^2 = \frac{1 - (4 - \tau_1)c_l^2 - (1 - \tau_1)\zeta c_l}{(1 - \tau_1)(1 - 6c_l^2 - 3\zeta c_l)} \quad \text{for } v_i \quad i \in \{1, 3\},$$

$$c_{\sigma_2}^2 = \frac{1 - (4 - \tau_2)c_l^2 - (1 - \tau_2)\zeta c_l}{(1 - \tau_2)(1 - 6c_l^2 - 3\zeta c_l)} \quad \text{for } v_i \quad i \in \{2, 4\}, \quad (39)$$

where we introduce the following notation

$$\tau_1 = \frac{A_1}{A_3}, \quad \tau_2 = \frac{A_2}{A_3}, \quad \zeta = \frac{\Delta}{\Theta}.$$

These relationships lead us to the following family of curves

$$c_{\sigma_1} = c_{\sigma_1}(c_l; \tau_1), \quad c_{\sigma_2} = c_{\sigma_2}(c_l; \tau_2)$$

whose graph is studied in the Cartesian plane  $O_{c_l c_{\sigma}}$ .

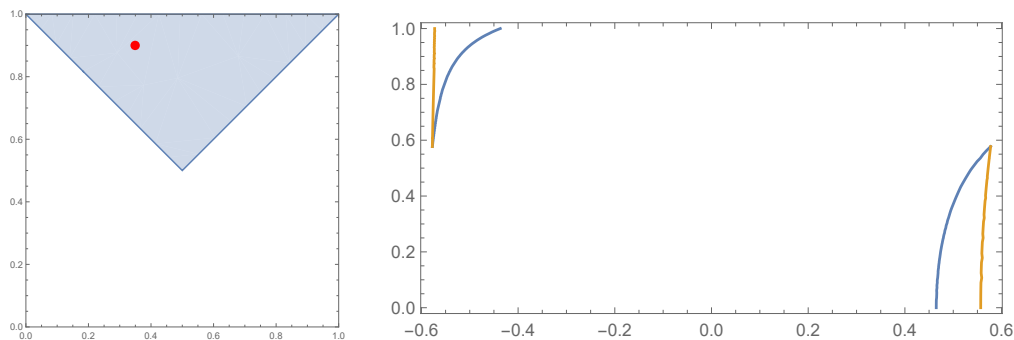


**Fig. 6** (Left) triaxiality region with  $\tau_1 = 0.35$  and  $\tau_2 = 0.9$ . (Right) Curves  $c_{\sigma_1}$  and  $c_{\sigma_2}$  restricted to interval  $[0, 1]$  for  $\zeta = 0.7$ .

Notice that the triaxiality of  $B_1$  is encapsulated in the ratios  $\tau_1$  and  $\tau_2$  respecting some conditions as  $0 < \tau_1 < \tau_2 < 1$  and  $1 < \tau_1 + \tau_2$ . On figure 6 we distinguish curves of equilibria. A complete analysis of these curves is a work on progress in [6].

A partial study of the triaxiality role is presented now in more detail due to the important effects produced on the inclinations of  $c_\sigma$  and  $c_l$  for this particular equilibria. Some important restrictions for the sake of simplicity must be considered. We restrict the domain of  $c_l$  to  $0 < c_l < 1/\sqrt{3}$  and use the following nomenclature:

$c_l^*$  is the  $c_l$ -intercept value of the curve  $c_{\sigma_1}$ , i.e.  $0 = c_{\sigma_1}(c_l^*; \tau_1)$  and  $c_l^{**}$  is the  $c_l$ -intercept value of the curve  $c_{\sigma_2}$  respectively, namely

$$c_l^* = \frac{\zeta(1 - \tau_1) - \sqrt{\zeta^2(1 - \tau_1)^2 - 4(\tau_1 - 4)}}{2(\tau_1 - 4)}, \quad c_l^{**} = \frac{\zeta(1 - \tau_2) - \sqrt{\zeta^2(1 - \tau_2)^2 - 4(\tau_2 - 4)}}{2(\tau_2 - 4)}.$$

Within our restriction and fixing a certain inclination  $\tilde{c}_l$ , we distinguish three regions:

- $\tilde{c}_l \in (0, c_l^*)$ : No equilibria is found for this fixed inclination.
- $\tilde{c}_l \in (c_l^*, c_l^{**})$ : One equilibrium found. As we notice in figures 7 and 8 (central) for a fixed inclination on this region we find one  $c_\sigma$  value that guarantee us an equilibrium.
- $\tilde{c}_l \in (c_l^{**}, 1/\sqrt{3})$ : Two equilibria found. Figures 7 and 8 (right) show that for a fixed inclination we find two  $c_\sigma$  values that guarantee us equilibrium.

Moreover in figures 7 and 8 (left) we included a representation of the triaxiality region.

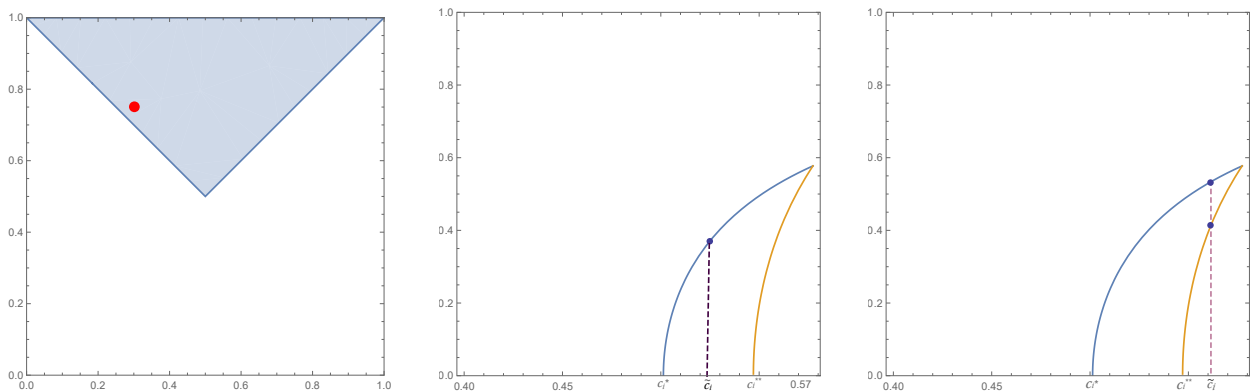


**Fig. 7** Parameters:  $\zeta = 0.2, \tau_1 = 0.3, \tau_2 = 0.75$ .

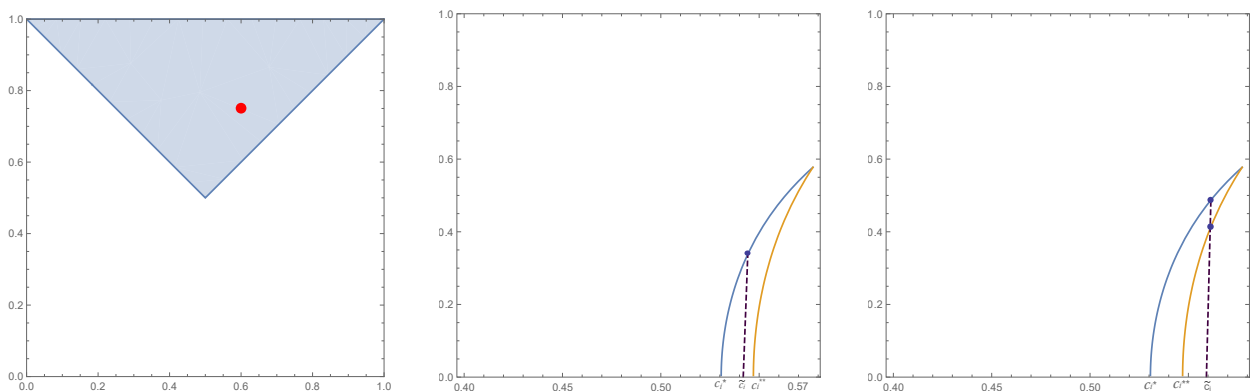


**Fig. 8** Parameters:  $\zeta = 0.2, \tau_1 = 0.6, \tau_2 = 0.75$ .

As we observe the triaxial shape of  $B_1$  acquires a fundamental role in the amplitude of the different regions of equilibria. Notice that the mentioned amplitude is also affected by the ratio  $\zeta$ . From a more detail study we conclude that this situation is robust enough even for values of  $\zeta > 1$ .

- *Fixed  $v$  and  $\psi$ . Invariant 2-tori  $\mathbb{T}^2(\theta, \delta)$  and periodic orbits.*

Working on the subsystems  $(\dot{r}, \dot{R})$ ,  $(\dot{v}, \dot{N})$  and  $(\dot{\psi}, \dot{\Psi})$  under an inclined equilibria and  $(1 - 3c_\sigma^2) = 0$  along with the following initial value problem, we obtain an equilibrium which guarantee us the existence of an orbit of constant radius within the invariant 2-tori  $\mathbb{T}^2(\theta, \delta)$ ,

$$\begin{aligned} R = 0, \quad r = \frac{\Theta^2}{\kappa}, \quad v = v_i, \\ 1 - 3c_\sigma^2 = 0, \quad c_i^2 = \frac{1}{3} \left[ 1 - q \left( \frac{A_3 - A_i}{A_3 A_i} \right) \frac{8\Delta^2 \Theta^6}{3\alpha \kappa^4} \right]. \end{aligned} \quad (40)$$

This particular inclination of  $\sigma$  provides us a body-inclined equilibria and leads us to recover in (16) the Kepler problem formulation. Moreover, it also guarantees us the existence of orbits within  $\mathbb{T}^2(\theta, \delta)$ .

Particularly the variation of the remainder angles are given by:

$$\dot{\theta} = n_\theta = \frac{\Theta}{r^2}, \quad (41)$$

$$\dot{\delta} = n_\delta = q\Delta \left( \frac{2A_3 + A_i}{3A_3 A_i} \right). \quad (42)$$

Notice that these mean motions for  $\theta$  and  $\delta$  provide us periodic orbits within  $\mathbb{T}^2(\theta, \delta)$ .

### 4.3 Body-Perpendicular equilibria

Along this section we study the equilibria obtained under a fixed inclination of the  $\sigma$  angle which determine the relative position of the rotational and body planes. In particular we consider  $c_\sigma = 0$  inclination dubbed as body-perpendicular equilibria. It is straightforward that  $N = 0$  is equivalent to have a perpendicular inclination. Observe that some of the perpendicular equilibria study on this section present critical inclination. Note that not likewise the inclined equilibria, the body-perpendicular equilibria allow a free regime of  $\Delta$ .

- *Fixed  $v$ . Invariant 3-tori  $\mathbb{T}^3(\theta, \psi, \delta)$ .*

Examining the subsystems  $(\dot{r}, \dot{R})$  and  $(\dot{v}, \dot{N})$  under a perpendicular inclination  $c_\sigma = 0$  along with the following initial value problem we obtain an equilibrium which guarantees us the existence of an orbit of constant radius within the invariant 3-tori  $\mathbb{T}^3(\theta, \psi, \delta)$

$$\begin{aligned} R = 0, \quad r = \frac{\Theta^2}{2\kappa} + \sqrt{\frac{\Theta^4}{4\kappa^2} - \frac{3\alpha(1 - 3c_i^2)}{16}}, \\ v = v_i, \quad N = 0. \end{aligned} \quad (43)$$

Observe that the radius obtained is according to [11] when the triaxial body tends to be axial-symmetric.

Worth noting is that when the orbital and the rotational planes present a critical inclination, i.e.  $1 - 3c_i^2 = 0$ , the formula for the radius is simplified to  $r = \Theta^2/\kappa$ . Notice that by analyzing (18) and (19) it can be concluded that there is no a simultaneous equilibrium for  $\delta$  and  $\psi$ . As such, we continue studying the existence of 2-tori originated by fixing each one of the remaining angles individually.

- *Fixed  $v$  and  $\delta$ . Invariant 2-tori  $\mathbb{T}^2(\theta, \psi)$ .*

Taking into account the subsystems  $(\dot{r}, \dot{R})$ ,  $(\dot{v}, \dot{N})$  and  $(\dot{\delta}, \dot{\Delta})$  under a perpendicular inclinations  $c_\sigma = 0$  and  $(1 - 3c_i^2) = 0$  along with the following initial value problem we obtain an equilibrium which guarantee us the existence of an orbit of constant radius within the invariant 2-tori  $\mathbb{T}^2(\theta, \psi)$

$$r = \frac{\Theta^2}{\kappa}, \quad R = 0, \quad v = v_i, \quad N = 0, \quad (44)$$

$$\Delta q \left( \frac{1}{A_i} \right) - \frac{3\alpha\kappa}{8} \left[ \frac{c_i(c_i + \frac{\Delta}{\Theta})}{\Delta r^3} \right] = 0, \quad c_i = \pm\sqrt{1/3}.$$

Notice that this equilibrium has the same constant radius as the one obtained for a critical inclination, therefore we interpret that for this equilibrium  $c_\sigma = 0$  confine the motion of our orbit within the invariant  $\mathbb{T}^2(\theta, \psi)$ .

The remainder angles are given by:

$$\dot{\theta} = n_\theta = \frac{\Theta}{r^2} - \frac{3\alpha\kappa}{8} \frac{c_i(c_i + \frac{\Theta}{\Delta})}{\Theta r^3}, \quad (45)$$

$$\dot{\psi} = n_\psi = \frac{3\alpha\kappa}{8} \frac{c_i\Psi}{\Delta\Theta r^3}. \quad (46)$$

- *Fixed v. Invariant 2-tori*  $\mathbb{T}^2(\theta, \delta)$ .

Analyzing the subsystems  $(\dot{r}, \dot{R})$ ,  $(\dot{v}, \dot{N})$  and  $(\dot{\psi}, \dot{\Psi})$  under  $c_\sigma = 0$  and  $c_i = 0$  along with the following initial value problem we find an equilibrium and therefore an orbit within the invariant 2-tori  $\mathbb{T}^2(\theta, \delta)$ .

$$R = 0, \quad r = \frac{\Theta^2}{2\kappa} + \sqrt{\frac{\Theta^4}{4\kappa^2} + \frac{3\alpha}{16}}, \quad (47)$$

$$v = v_i, \quad N = 0.$$

The expression for the remainder angles are:

$$\dot{\theta} = n_\theta = \frac{\Theta}{r^2}, \quad (48)$$

$$\dot{\delta} = n_\delta = \left( \frac{\Delta q}{A_i} \right). \quad (49)$$

Consequently the mean motions of  $\theta$  and  $\delta$  provide us periodic orbits withing  $\mathbb{T}^2(\theta, \delta)$ .

## 5 On the classical families of relative equilibria

In general, classical relative equilibria of the roto-orbital dynamics associated with a rigid body in circular orbit [16, 21, 22] are not reflected in our analysis, since they require particular inclinations of the fundamental planes involved leading to angles singularities. For instance, the solutions usually designated as *float* implies that the orbital, rotational and body planes are coplanar. Thus, several of the angular canonical variables are not defined and we should switch to another chart including this possibility. Indeed, this situation is associated to any relative equilibria in which the rotation is around axis  $b_3$ .

Next, we consider some special configurations. Let  $\iota$  be fixed to  $\pi/2$ , then we find relative equilibria among the family of perpendicular type ( $\sigma = \pi/2$ ) in which the spin axis lies in the orbital plane. When we set initial

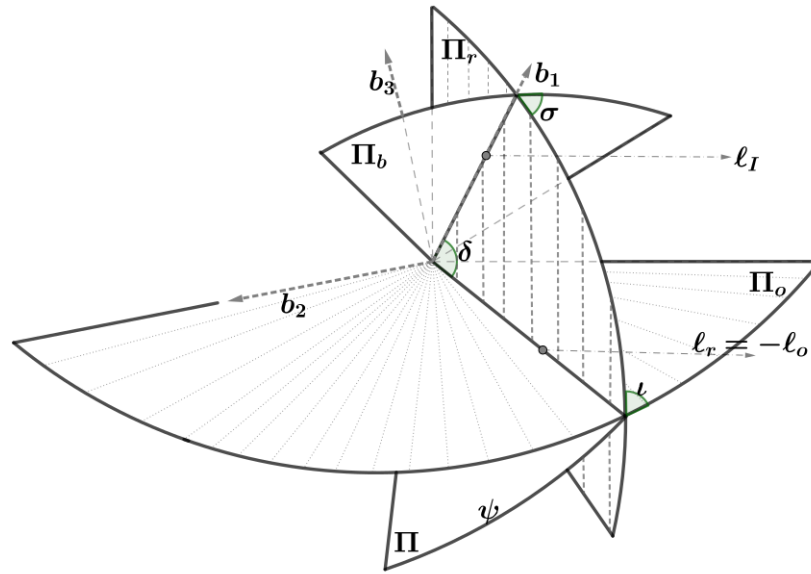


**Fig. 9** Special relative equilibria of the body-perpendicular type with  $\nu = \pm n\pi$ .

conditions for  $\sigma = \pi/2$  and  $\psi$  fixed, *i. e.*, body-perpendicular relative equilibria among the family  $\mathbb{T}^2(\theta, \delta)$ , the body is spinning around  $b_1$  (for  $\nu = \pi/2 \pm n\pi$ ) or  $b_2$  (for  $\nu = \pm n\pi$ ). In both cases, the spin-axis is in the intersection of the orbital and body planes. Figure 9 provides an illustration of the situation described by considering a reference frame attached to the orbital plane. Note that the angles  $\theta$  and  $\delta$  are moving at a constant rate. Thus, the spin axis  $b_2$  or  $b_1$  defines the invariant direction of the rotational angular momentum in the space frame.

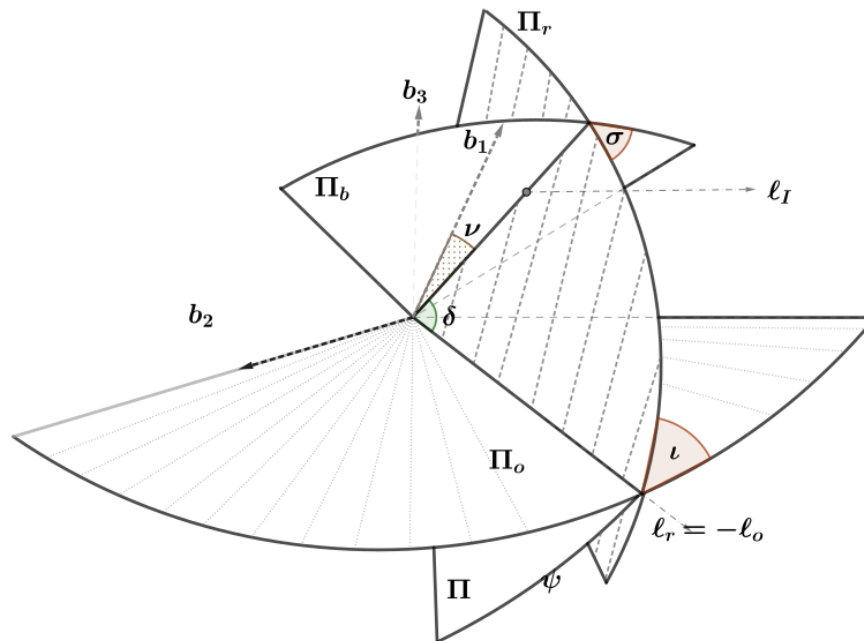


**Fig. 10** Special relative equilibria of the body-inclined type.

These relative equilibria are similar to the types *arrow* and *spoke* reported by [16, 21] inasmuch as the spin

axis lies in the orbital plane. However, in order to recover the actual classical relative equilibria, we should allow the angle  $\psi$  to vary. Thus, we consider body-inclined relative equilibria when  $\sigma + \iota = \pm\pi$ . Then, since  $v$  is also fixed, one may choose this angle in such a manner that  $b_1$  (or  $b_2$ ) lies in the orbital plane. Nonetheless, in this configuration  $\psi$  and  $\theta$  evolves at constant rate giving the classical *arrow* and *spoke* types at particular frequencies. See figure 10 for a geometric view of this instance.

As a final remark, we would like to point out that, a complete identification of the classical families of relative equilibria involves the use of a complete set of charts, which cover the case in which the axis  $b_3$  is allowed to be the spin-axis.

## 6 Conclusions and future work

An intermediary model has been presented considering the triaxial version of the one introduced in [11]. The numerical simulations assess the validity of the model for the case of a fast rotating body. Although, more exhaustive experiments are necessary to establish bounds for its applicability. Moreover, our experiments show the influence of the triaxiality reporting a marked degradation in the precision of the fast angles, though the radial distance and slow angles remain to be approximated with high accuracy after one orbital period. Nevertheless, the evaluation of a slow rotation regime is part of our ongoing research.

We also investigate the relative equilibria of the model finding families that depart from the equilibria of the free rigid body and the classical equilibria reported in the literature. Yet, some of these equilibria are recovered in our setting and we give a detailed geometric description of how to identify them. A complete searching of classical equilibria in our setting requires the use of several charts. The role of the triaxial shape of the body is studied for some equilibria, showing partially how the triaxiality influences the inclinations which lead to equilibria. The integrability of our model and the stability of the equilibria obtained are parts of a further research.

## Acknowledgment

Support from Research Agencies of Spain and Chile is acknowledged. They came in the form of research projects MTM2015-64095-P and ESP2017-87271-P, of the Ministry of Science of Spain and from the project 11160224 of the Chilean national agency FONDECYT.

## APPENDIX

Though the argument of the node of the orbital and rotational planes are not included in the set of canonical variables, neither the inclinations of the fundamental planes or eccentricity, they are connected to them. By zooming Figure. 1, we obtain Figure. 11, which help us in obtaining some relations.

Using basic formulas of spherical trigonometry, the following relation can be derived

$$\begin{aligned}
 \cos I_{\Theta} &= \cos I_o \cos I + \sin I_o \sin I \cos \psi, & \sin I_{\Theta} &= +\sqrt{1 - \cos^2 I_{\Theta}}, \\
 \cos \alpha &= \frac{\cos I_o \cos I_{\Theta} - \cos I}{\sin I_o \sin I_{\Theta}}, & \sin \alpha &= \frac{\sin I}{\sin I_{\Theta}} \sin \psi, \\
 \cos(\phi - h) &= \cos \alpha \cos \psi + \sin \alpha \sin \psi \cos I_o, & \sin(\phi - h) &= \frac{\sin I_o}{\sin I_{\Theta}} \sin \psi,
 \end{aligned} \tag{A1}$$

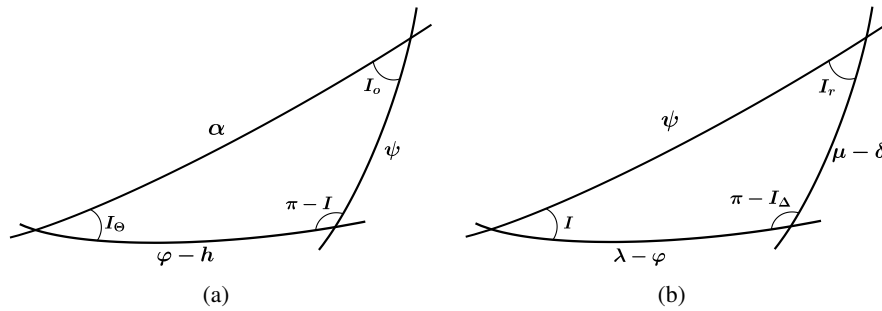


**Fig. 11** Spherical triangles involved in the problem.  $\alpha$  is the angle between the two nodes of the orbital plane. (a) Triangle formed by the orbital angular momentum plane, the total angular momentum plane and the reference plane. (b) Triangle formed by the rotational angular momentum plane, the total angular momentum plane and the reference plane.

while for the case of Fig. 11(b), we can write

$$\begin{aligned}
 \cos I_{\Delta} &= \cos I_r \cos I - \sin I_r \sin I \cos \psi, & \sin I_{\Delta} &= +\sqrt{1 - \cos^2 I_{\Delta}}, \\
 \cos(\lambda - \phi) &= \frac{\cos I_r - \cos I \cos I_{\Delta}}{\sin I \sin I_{\Delta}}, & \sin(\lambda - \phi) &= \frac{\sin I_r}{\sin I_{\Delta}} \sin \psi, \\
 \cos(\mu - \delta) &= \cos(\lambda - \phi) \cos \psi + \sin(\lambda - \phi) \sin \psi \cos I, & \sin(\phi - h) &= \frac{\sin I}{\sin I_{\Delta}} \sin \psi,
 \end{aligned} \tag{A2}$$

## References

- [1] Andoyer, M. H.: *Cours de Mécanique Céleste*. Gauthier-Villars, Paris, 57 (1923)
- [2] Arribas, M.: *Sobre la dinámica de actitud de satélites artificiales*. PhD, Universidad de Zaragoza, 149 (1989)
- [3] Beletskii, V. V.: *Motion of an artificial satellite about the center of mass*. Israel Prog. for Scientific Trans., Jerusalem (1966)
- [4] Boué, G., Laskar, J.: Spin axis evolution of two interacting bodies, *Icarus*. 201, 2, 750–767 (2009), doi.org/10.1016/j.icarus.2009.02.001
- [5] Buono, L., Laurent-Polz, F., Montaldi, J.: In *Geometric Mechanics and Symmetry: The Peyresq Lectures*. J. Montaldi and T. S. Ratiu, eds, Cambridge University Press. Berlin, 357-402 (2005)
- [6] Cantero, A.: *Mathematical Models for the Full Gravitational 2-Body Problem. A Perturbative Scheme by Stages*. PhD thesis, Universidad de Murcia. In Progress.
- [7] Chernousko, F. L.: On the motion of a satellite about its center of mass under the action of gravitational moments. *Journal of Applied Mathematics and Mechanics* 27, 3, 708-722 (1963)
- [8] Cochran, J. E.: Effects of Gravity-Gradient Torque on the Rotational Motion of a Triaxial Satellite in a Precessing Elliptic Orbit. *Celestial Mechanics* 6, 127-150 (1972)
- [9] Crespo, F.: *Hopf fibration reduction of a quartic model. An application to rotational and orbital dynamics*. PhD Thesis, Universidad de Murcia, 208 (2015)
- [10] Crespo, F.J., Ferrer, S. Roto-orbital dynamics of a triaxial rigid body around a sphere. *Relative equilibria and stability*, *Advances in space research* 61, 2725-2739 (2018)
- [11] Crespo, F., Molero, F.J., Ferrer, S., Scheeres, D.J. A radial axial-symmetric intermediary model for the roto-orbital motion, *Journal of Astronautical Sciences* 65, 1-28 (2018). doi: [10.1007/s40295-017-0121-9](https://doi.org/10.1007/s40295-017-0121-9)
- [12] de Moraes, R., Cabette, R., Zanardi, M., Stuchi, T., Formiga, J.: Attitude stability of artificial satellites subject to gravity gradient torque. *Celest. Mech. Dyn. Astr.* 104, 337-353 (2009). doi: [10.1007/s10569-009-9216-3](https://doi.org/10.1007/s10569-009-9216-3)
- [13] Dellnitz, M., Melbourne, I., Marsden, J.E.: Generic bifurcation of Hamiltonian vector fields with symmetry. *Nonlinearity* 5, 979-996 (1992)
- [14] Deprit, A.: The elimination of the parallax in satellite theory. *Celestial Mechanics* 24, 2, 111-153 (1981)
- [15] Deprit, A.: Elimination of the nodes in problem of N bodies. *Celestial Mechanics* 30, 2, 181-195 (1983)
- [16] Duboshin, G. On one particular case of the problem of the translational-rotational motion of two bodies. *Soviet Astronomy*, 3:154. (1959)
- [17] Ferrándiz, J. M., Sansaturio, M. E: Elimination of the nodes when the satellite is a non spherical rigid body. *Celestial Mechanics* 46, 307–320 (1989)

- [18] Ferrer, S., Lara, M.: On Roto-Translatory Motion: Reductions and Radial Intermediaries. *The Journal of the Astronautical Sciences* 59, 1-2, 21-39 (2012)
- [19] Ferrer, S., Molero, F. J.: Intermediaries for Gravity-Gradient Attitude Dynamics I. Action-angle variables. *Advances in the Astronautical Sciences* 153, 293-312 (2nd IAA Conference on Dynamics and Control of Space Systems. Roma. Italy. 24-26 March 2014)
- [20] Hughes, P. C.: *Spacecraft Attitude Dynamics*. Dover Public Inc, New York (1986)
- [21] Kinoshita, H.: Stationary Motions of an Axisymmetric Body around a Spherical Body and Their Stabilities. *Publications of the Astronomical Society of Japan* 22, 383-403 (1970 )
- [22] Kinoshita, H.: Stationary Motions of a Triaxial Body and their Stabilities. *Publications of the Astronomical Society of Japan* 24, 409-417 (1972)
- [23] Ferrer, S. and Lara, M. On roto-translatory motion: Reductions and radial intermediaries. *The Journal of the Astronautical Sciences*, 59:21–39. (2012)
- [24] Lara, M., Ferrer, S.: Closed form perturbation solution of a fast rotating triaxial satellite under gravity-gradient torque. *Cosmic Research* 51, 4, 289-303 (2013). doi: [10.1134/S0010952513040059](https://doi.org/10.1134/S0010952513040059)
- [25] Lara, M., Gurfil, P.: Integrable approximation of  $J_2$ -perturbed relative orbits. *Celestial Mechanics and Dynamical Astronomy* 114, 229-254 (2012). doi: [10.1007/s10569-012-9437-8](https://doi.org/10.1007/s10569-012-9437-8)
- [26] MacCullagh, J.: On the rotation of a solid body. *Proceedings of the Royal Irish Academy* 2, 520-545 (1840)
- [27] Scheeres, D.: *Orbital Motion in Strongly Perturbed Environments: Application to Asteroid, Comet and Planetary Satellite Orbiters*. Jointly published with Praxis Publishing, UK, 390 (2012)
- [28] Scheeres, D.: Minimum energy configurations in the N-body problem and the celestial mechanics of granular systems. *Celest. Mech. Dyn. Astr.* 113, 291-320 (2012). doi: [10.1007/s10569-012-9416-0](https://doi.org/10.1007/s10569-012-9416-0)
- [29] Sidi, M. J.: *Spacecraft Dynamics and Control*. Cambridge Aerospace Series (2000)
- [30] Soler, A.: *Intermediarios radiales del movimiento roto-traslatorio de satélites artificiales* PhD Thesis, Universidad de Murcia (2013)
- [31] Wang, Y., Xu, S., Zhu, M.: Stability of relative equilibria of the full spacecraft dynamics around an asteroid with orbit-attitude coupling. *Advances in Space Research* 53, 1092-1107 (2014)
- [32] Wilson, C.: *The Hill-Brown Theory of the Moon's Motion*. Springer, 332 (2010)
- [33] Zanardi, M., Silva, W., Formiga, J., Stuchi, T., Cabette, R.: Stability analysis of the spacecraft attitude with canonical variables. *Proceedings of the 23<sup>th</sup> International Symposium on Space Flight Dynamics — 23<sup>th</sup> ISSFD, Pasadena, USA* (2013)